Finite element analysis of planar stress anisotropy and thermal behavior in thin films

by K. F. Young

To show the capability and diversity of finite element analysis, we calculate three-dimensional planar anisotropic stress distributions for various thin-film geometries and materials in response to thermal and electrical stimuli, for specific boundary conditions. The simulated residual film stresses are verified with acoustic microscopy measurements, substrate flexure measurements, and the use of thermal environment techniques. Simple shapes are analyzed as building blocks for more complex structures. Effects of nonlinear electrical resistance are also analyzed.

1. Introduction

Finite element analysis (FEA) is a powerful tool [1] that can be used to describe the thermal, electrical, magnetic,

[®]Copyright 1990 by International Business Machines Corporation. Copying in printed form for private use is permitted without payment of royalty provided that (1) each reproduction is done without alteration and (2) the *Journal* reference and IBM copyright notice are included on the first page. The title and abstract, but no other portions, of this paper may be copied or distributed royalty free without further permission by computer-based and other information-service systems. Permission to *republish* any other portion of this paper must be obtained from the Editor.

and stress-related characteristics of thin-film magnetic recording heads. Presented here are aspects of how this tool operates and how it is used to achieve a fundamental understanding of these characteristics. This understanding may then be applied to magnetic domain instability and electromigration mechanisms, in order to increase the performance and reliability of magnetic recording heads. As magnetic recording densities increase, domain instabilities in recording heads due to magnetostrictive effects caused by planar anisotropic stress conditions are no longer negligible. Therefore, it becomes ever more desirable to characterize the fundamental behavior of stresses (mechanical and thermal) in thin-film structures and apply that knowledge to improve real devices. Computer simulation of planar stress anisotropy and thermal behavior assists us to make substantial performance improvements and increase device lifetimes while reducing extensive prototyping involving variation of geometrical and material properties.

The finite element application program ANSYS¹ is used for all of the analyses presented here. Since we are concerned with thin films rather than bulk materials in this work, we use the phrases "stress anisotropy" or

¹ ANSYS is a trademark of Swanson Analysis Systems, Inc., P.O. Box 65, Johnson Rd., Houston, PA 15342.

"anisotropic stress" below to refer to the anisotropy of the stress components that lie in (or nearly in) the plane of the film.

Finite element analyses are generally structured in three parts: preprocessing, equation solution, and postprocessing.

Preprocessing comprises the following:

- Mesh generation—specifying the location of nodes and using those points to define the finite elements (grouping into unit cells).
- Material specification—defining regions (collections of elements) and the parameters of the materials in those regions
- · Specification of boundary conditions and stimuli.

In the equation solution portion of finite element analysis, matrix formulation and triangularization are accomplished. The numerical solution yields the values of displacements, stresses, temperatures, and other variables.

Postprocessing involves interactive techniques for graphically viewing and numerically listing the results of the calculations.

We describe FEA techniques and their verification in the analyses of mechanical stress in three examples:

- An etched slot in a thin film.
- · A rectangular section of a thin film.
- A thin film deposited on a circular wafer (disk).

In addition, two examples deal with FEA stress analysis applied to magnetic recording heads:

- Anisotropic stress and magnetoelastic energy in an inductive head.
- Electrical/thermal effects in a magnetoresistive (MR) head.

In Sections 2–6, we perform the three-part general form of analysis on the five examples chosen and describe significant features of each example. Typical FEA techniques are used. For instance, to ensure that the approximate numerical solution is close enough to the solution of the differential equations, we increase mesh density and extend the mesh (for infinitely large regions) until negligible changes in stress or temperature results are observed.

Thin films acquire residual stress from the deposition process, part of which is due to intrinsic stress occurring during the deposition itself and part to thermal expansion mismatch of the materials. Since stresses normal to edges and surfaces must be zero, the residual stress field may be considered to be a combination of a large, uniform,

Table 1 Mechanical constants of materials used in analyses of Sections 2–5 (handbook values for bulk, isotropic materials).

Material	Modulus of elasticity E_{γ} (× 10^{12} Pa)	Thermal expansion α_T (× 10^{-6} K ⁻¹)	Poisson's ratio v
Alumina	0.345	6.4	0.25
Copper	0.117	16.5	0.33
Nickel-iron (Permalloy)	0.207	12.2	0.30
Photoresist	0.001	140	0.20
Silicon	0.107	4.7	0.30

isotropic, in-plane stress field with a smaller anisotropic stress field. The anisotropic stress plays a key role in influencing magnetic domain behavior, as we mention in Section 5. For the purpose of our calculations in Sections 2-4, we assume that the stress is due to a delta strain stimulus arising from a uniform temperature change of the two layers (film and substrate), which have different thermal expansion coefficients. In Section 5, the assumption is extended to a multiple-layer structure. The resulting anisotropic stress pattern is formed by the geometric shapes and the moduli of elasticity of the materials. In general terms, we may say that a uniform temperature change with different material properties results in an anisotropic stress distribution. The usefulness of this technique is supported by the experiments discussed in the following sections.

Table 1 lists the mechanical constants for the materials used in the analyses of Sections 2-5.

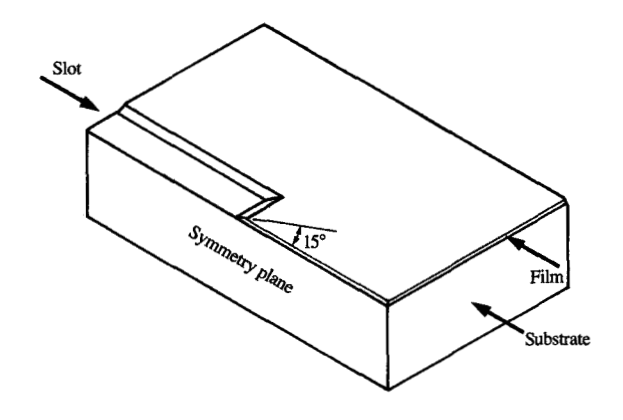
Each mesh is generated so that the mesh density is greater in the regions having sharp features. Where the stress gradients are highest and stress contours have the most curvature, a more closely spaced finite element mesh will yield calculated stress values that better approximate the continuum of nature. Isoparametric solid elements are used for the finite element meshes.

One technique for analyzing real devices, which have edges, corners, tapers, fillets, and even more complex geometric features, is to characterize a variety of simple features and then use them as building blocks to attain knowledge of complex structures. We expect to accomplish this in the near future.

2. Etched slot in thin film

One such simple feature is an etched slot—a long, narrow, rectangular portion of a thin film removed by an etching process. As a result of the removal, an anisotropic stress field arises along the edges of the slot. Calculations of this field are given in this section and compared with acoustic microscope images.

Figure 1 shows the three-dimensional geometry used in the analysis of the etched slot in the film. The etching



Three-dimensional geometry of an etched slot in a thin film deposited on a substrate.

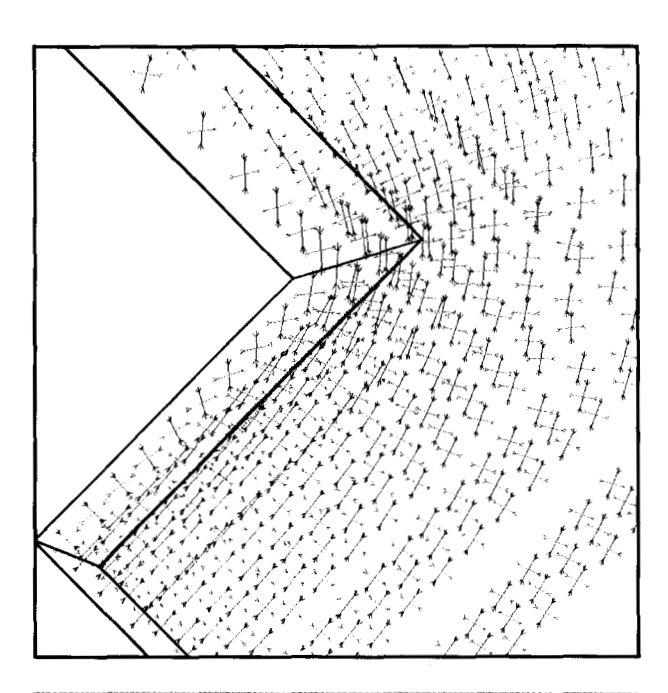


Figure 2

Calculated (by finite element analysis) principal stress vector field for the tip of a 400- μ m-wide slot etched in a thin film, isometric view.

process leaves a wall sloping at about 15 degrees to the horizontal, and this sloping wall is included in the finite element analysis. We experiment upon a 400- μ m-wide slot etched in a 15- μ m-thick layer of sputtered alumina

on a glass substrate. Because of the longitudinal symmetry, only half of the mesh has to be calculated, thereby requiring approximately one-half the computational resources.

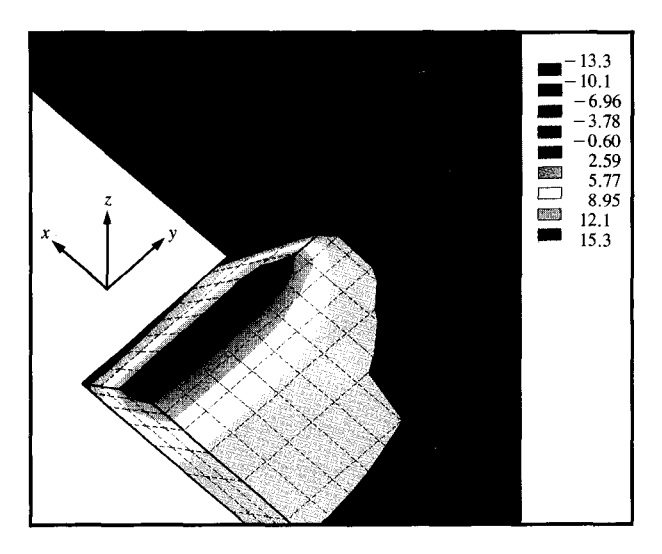
Figures 2–4 show the results of calculations for the half of the etched slot shown in Figure 1. Although the analyses are performed for the complete configuration of Figure 1, only the thin film is shown. All three figures are isometric views.

The calculated principal stresses are plotted in vector form at the centroid of each element in Figure 2. For each element, two of the three principal stresses are shown (the third is generally negligible for planar structures). The vector representing the maximum of the compressive principal stresses is colored blue; the other visible principal stress vector is colored green. The triplet patterns of vectors (especially visible in the lower righthand area of the figure) are due to the three-elementthick mesh; the triplet patterns merge with others where the mesh is denser. Notice that the field of blue vectors "flows" around the corner of the slot. If there are no external applied forces, stress components normal to a surface must vanish as they approach that surface. This phenomenon can be seen in the tendency of the stress vectors to align parallel to the edges and surfaces in Figure 2. These represent the planar stress anisotropy that is analyzed in this work.

The calculated differences between the X and Y components (aligned with the global coordinate system of the slot) of the planar stresses, $S_x - S_y$, are shown in **Figure 3**. This difference in stress is the stress anisotropy. The uniform, planar isotropic stress state of an infinite plane has zero stress anisotropy. This zero anisotropic stress field is represented by the broad, uniform field of green that is far from the slot edges. The two edges have opposite signs of stress anisotropy, because the components normal to the edge vanish and the slot edges are orthogonal. The stress anisotropy has its maximum values at the edges, except for the corner.

Figure 4 is the calculated sum of planar stresses, $S_x + S_y$, which is used to correlate simulations with measurements, as discussed below. The stress is uniform in the far field (featureless area of the film, beyond that shown in Figure 4). In this region, $S_x + S_y$ is approximately equal to twice the value of the isotropic compressive stress (2 × -40 MPa). The sum of the stresses is less compressive along the edges and away from the corner and (for the specific mesh density chosen, which is suitable for our other calculations) rises to 102 MPa in the infinitely sharp corner near the interface of film and substrate.

The measurement, on a microscopic scale, of planar stress sums and differences in thin films can be accomplished by observing the influence of stress upon



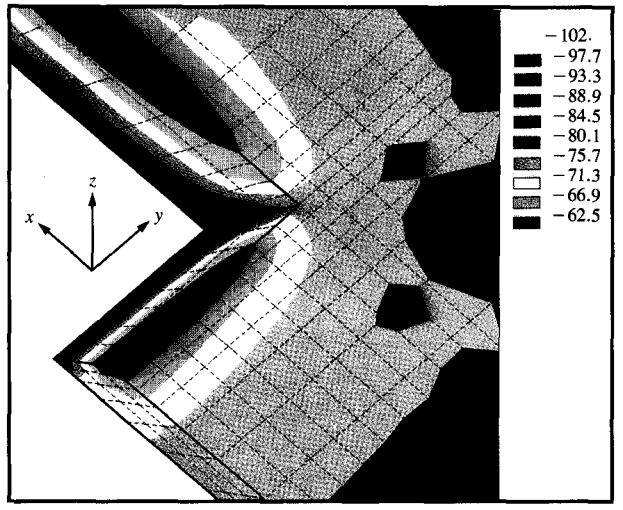


Figure 3

Calculated stress differences, $S_x - S_y$, for etched slot, isometric view (MPa).

Figure 4

Calculated stress sums, $S_x + S_y$, for etched slot, isometric view (MPa).

the acoustoelastic coefficients of a material. A highresolution, scanning, phase-measuring acoustic microscope (SPAM) was used by Meeks et al. [2] to image the near-surface residual stress field around a slot etched in sputtered alumina. Operating at 670 MHz, it has a resolution of 5–10 μ m. Figures 5 and 6 illustrate the use of the SPAM to map residual stress. Figures 5(a) and 6(a) show the finite element simulation of the difference of the stresses $(S_y - S_y)$ and the sum of the stresses $(S_x + S_y)$, respectively, at the end of the slot. (The slot corners are labeled A and B.) The views are orthogonal, seen from above. (Note that Figures 3 and 4 are *isometric* views of half of the etched slot.) Figures 5(b) and 6(b) show the experimental images of the same stress fields superimposed on a photomicrograph of the real slot. They compare well.

To calibrate the acoustic microscope, we determine the intrinsic macroscopic isotropic residual stress by measuring the curvature of the glass substrate. This measurement implies a value of (compressive) stress of -40 MPa. In the finite element calculation, a similar calibration is performed by applying a uniform temperature change to the bilayer structure. This is accomplished by adjusting the uniform temperature change until the far-field isotropic stress equals the value of -40 MPa. Having performed the calibration, we can extend the predictions of the FEA to other configurations without further calibration.

This one geometry, the etched slot, shows the extent to which edges, corners, and slopes can modify planar

isotropic stress to create various magnitudes and directions of stress anisotropy.

3. Rectangular section of film on substrate

To help us understand further the effects of edges and corners on anisotropic stress, a 3D analysis of a rectangular section of thin film on a large substrate is presented. (Such sections are of interest in the design of magnetic recording heads, where the film thickness and ratio of length to width are important.) As before, the stresses are delta-strain-driven because of a uniform temperature change in a structure with layers of different thermal expansion coefficients. Again, geometric shapes and moduli of elasticity determine the stress response. Because of the fourfold symmetry, only one-fourth of the structure has to be analyzed. The center of the film section is shown at the top of Figure 7, and a corner is shown at the bottom. In this example, a $2-\mu$ m-thick, $50-\mu m \times 60-\mu m$ nickel-iron film on a large alumina substrate is used. For the views of Figures 7 and 8, most of the substrate is removed, except for one row of substrate elements that is adjacent to the edge of the rectangular section. The finite element mesh chosen for the thin film in this case has two layers of elements.

Figure 7, like Figure 3, shows the differences in planar stress distribution components, $S_x - S_y$. Note the broad uniform field of green that represents the zero anisotropic stress far from the edges. As expected, the two edges have opposite signs of stress anisotropy, because the components normal to the edge must vanish and the

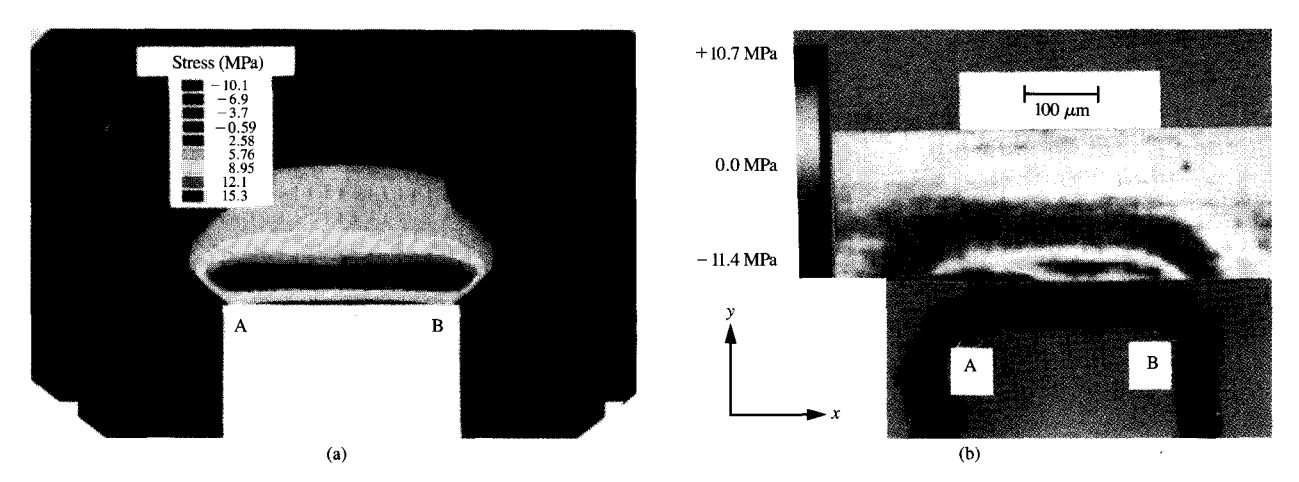


Figure 5

Calculated (a) and measured (b) stress differences for etched slot (viewed orthogonally from above).

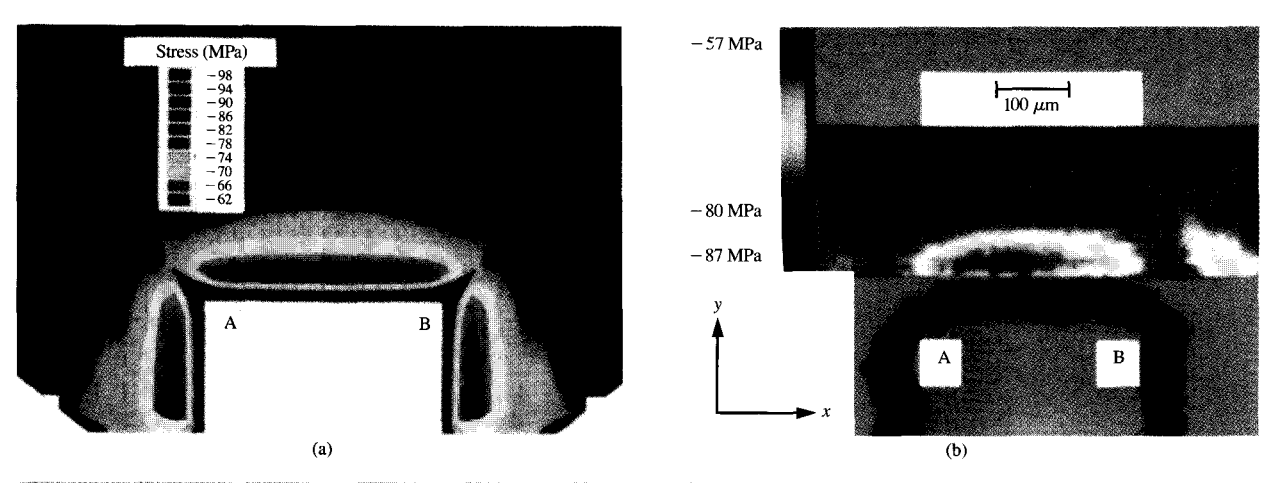


Figure 6

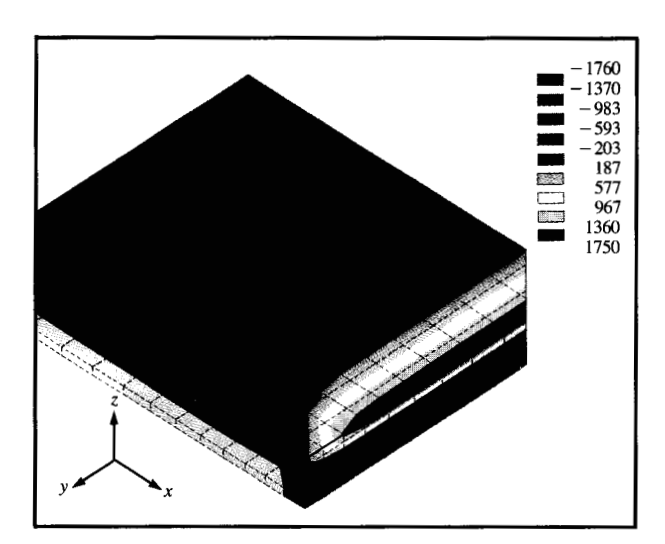
Calculated (a) and measured (b) stress sums for etched slot (viewed orthogonally from above).

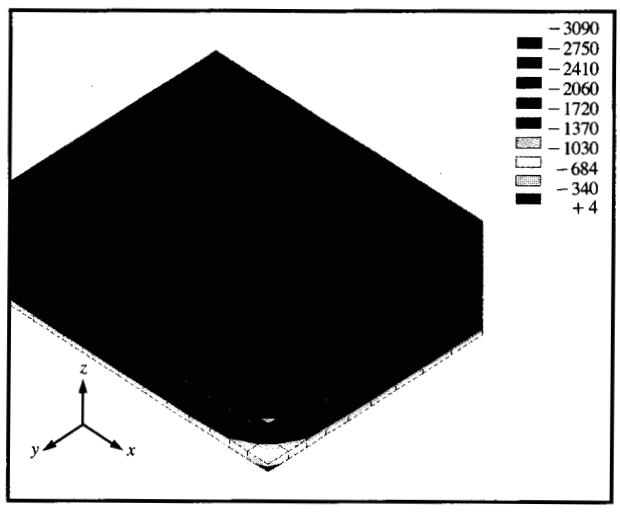
edges are orthogonal. The stress along both of the edges falls to zero as the corner is approached both along the surface and along the film thickness direction.

Figure 8 is an isometric view of the calculated maximum compressive principal stress. Note the broad, uniform field of blue that represents the isotropic planar stress far from the edges. As expected, the edge effects cause the stress to decrease as it nears the edge and to decrease more than twice as much as it nears the corner.

To further explore the stress behavior at the film edges, we construct a 2D model of the same rectangular section of film, with greater mesh density. Figure 9 shows the displaced mesh for such a 2D case, in which the

displacement, or strain, is scaled up by a factor of 10^4 . This exaggerated displacement helps us visualize the stress, which is proportional to the displacement (strain) by the modulus of elasticity ($E_{\rm Y}$, Young's modulus). Lacombe [3] analyzes a similarly displaced polyimide film; however, it is on a negligibly displaced silicon substrate. His ratio of Young's moduli of substrate to film is a factor of 37, whereas here it is 1.7 for alumina with a nickel-iron film. Although thermal mismatch strain may be large, the system stresses and displacements generated also depend upon the "spring constants" of the materials, so the net stress depends upon both factors. The calculated displacement shown in Figure 9 can be





Calculated stress differences, $S_{\rm x}-S_{\rm y}$, for rectangular sheet, isometric view (MPa).

Eletite.

Calculated maximum principal compressive stresses for rectangular sheet, isometric view (MPa).

verified qualitatively simply by constructing appropriate shapes of film and substrates from sheets of soft urethane foam. The "film" is compressed in the X (or Y) direction; contact cement is applied to the interface between "film" and "substrate"; the two materials are bonded; and the "film" is released from its compression. The resulting edge view of the two foam layers appears identical to the displacement shown in the figure.

Since the shapes dealt with thus far are simple, measurements and verification are not too difficult to implement. The finite element analysis of stress anisotropy can be extended, by varying geometries, materials, and boundary conditions, to simulate progressively more complex features of thin-film structures and processing steps.

4. Thin film on circular wafer

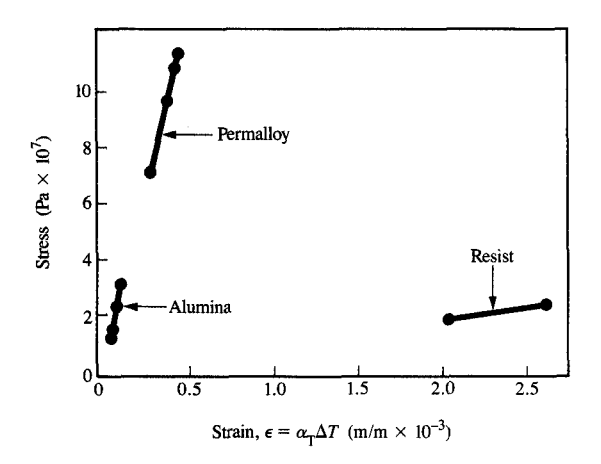
Deposition of thin films upon circular wafers causes the wafers to flex. In this work, FEA calculations of the isotropic stresses are verified by correlation with measurements. This verification technique is used, for example, in the work of Miyauchi et al. [4]. In this section, calculations are made to obtain the temperature vs. stress relationship. As discussed above, to the first order, a residually stressed wafer can be considered to be an unstressed one that has been exposed to a uniform temperature change. We denote by ΔT the change in uniform temperature required, according to the FEA calculation, to produce the same wafer deflection as that caused by residual stress in a real film. This relationship determination, which was performed in detail for ten

Figure 9

Calculated displacements of rectangular sheet, using 2D mesh (displacements multiplied by 10^4).

Permalloy, alumina, and photoresist films deposited on silicon substrates,² resulted in very good agreement.

² Depositions and measurements performed by W. Huang, IBM Storage Systems Products Division, San Jose, CA.



Calculated stress vs. strain (thermal expansion coefficient α_T multiplied by differential temperature ΔT).

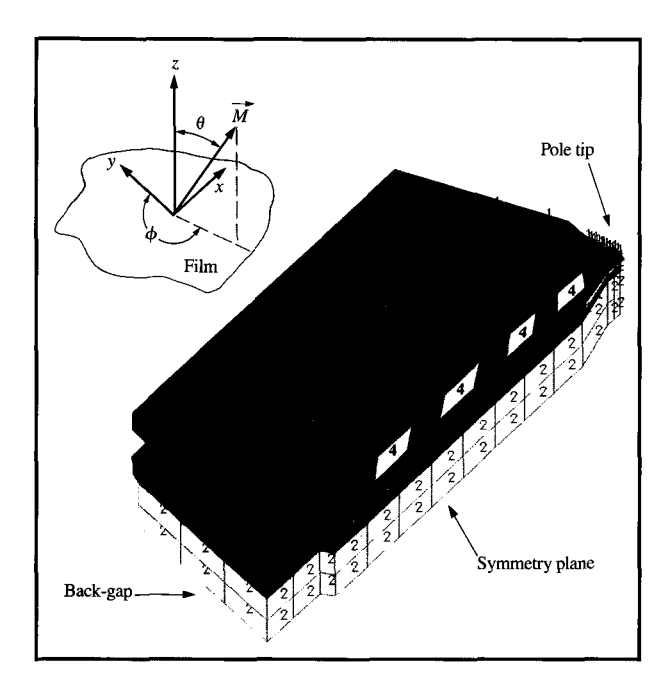


Figure 11

FEA mesh for a typical inductive head [layers: light blue (1) = metal (nickel-iron); yellow (2) = ceramic (alumina) substrate/undercoat; red (3) = photoresist; white (4) = copper].

An extension of the verification technique is shown in **Figure 10**, in which the stress is plotted against the strain. The strain is calculated by multiplying the thermal

expansion coefficient α_T by the difference in uniform temperature ΔT needed to bend the simulated wafer the same amount that the real wafer bends. The slope of the stress vs. strain line should be $E_Y/(1-\nu)$, a function of the modulus of elasticity E_Y and Poisson's ratio ν . As expected, the slopes match the respective material property values: Alumina (an oxide) has a somewhat higher slope than Permalloy (a metal), and both of them have much higher slopes than photoresist (a polymer).

This "calibration" is a necessary step to verify that the FEA calculations are valid for a simple geometry before extending them to more complex geometries.

5. Planar anisotropic stress and magnetoelastic energy in an inductive head

Anisotropic stress contributions to magnetoelastic energy can influence magnetic domain configurations in recording heads. It has been recognized that magnetic recording heads acquire residual stress from both fabrication steps and exposure to elevated temperatures. Calculations of anisotropic stresses and the roles of these stresses in magnetic domain formation have appeared in the literature (Koyanagi et al. [5] and Young [6]).

In this section, residual stress states are calculated by FEA for a typical recording head on the basis of its geometry, materials, and thermal history. In this initial analysis, decoupled elasticity field equations were used to assess the distribution of stress-induced magnetic anisotropy in the film.

When a recording head is subjected to a uniform temperature change in the simulation, the effect of the differences in thermal expansion coefficients simulates annealing. When, in the simulation, individual layers are set to different temperatures, the resultant stresses simulate the intrinsic stresses of their film deposition.

Figure 11 shows a typical mesh for simulating layers of alumina, nickel-iron, polymer insulation (photoresist), and copper coils. Because of symmetry, only half of the head need be analyzed; the symmetry plane is indicated in the isometric view of Figure 11.

Klokholm et al. [7] develop a functional relationship of magnetic anisotropic energy per unit volume of film, $E_{\rm k}$, to magnetization direction for polycrystalline thin magnetic films,

$$E_{\rm k} = \left[K_{\rm u} - \left(\frac{3}{2}\right)\lambda(S_{\rm x} - S_{\rm y})\right]\cos^2\phi\sin^2\theta,$$

where $K_{\rm u}$ is the field-induced uniaxial anisotropy constant, λ is the magnetostriction constant for cubic polycrystalline materials, θ is the polar angle of the magnetization vector \vec{M} from the normal of the film plane (the coordinate system is shown in Figure 11), and ϕ is the azimuthal angle that \vec{M} makes with the principal

stress axis. If S_x , S_y , and S_z are taken to be the principal stresses, the shear terms are absent ($S_{xy} = S_{yz} = S_{xz} = 0$). This relationship assumes that the principal stress axes are in the film plane ($\theta = \pi/2$), which is generally true except where there are significant geometric features such as tapers and curves.

The stable equilibrium condition exists where there are minima in the energy $E_{\rm k}$, which has a $\cos^2\phi$ dependence upon the magnetization direction ϕ in the plane of the film. Since $E_{\rm k}$ is negative, the minima occur at $\phi=0$ and π . Basically, these two "easy" magnetization directions lie along a line in opposite directions.

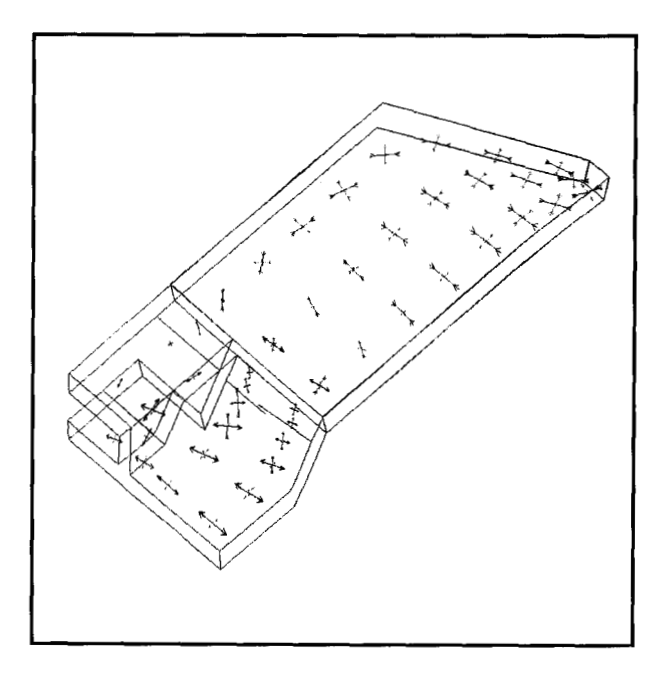
The vector plot of Figure 12, like Figure 2, displays the direction of the calculated principal stresses in the yoke region, as driven by thermal expansion mismatch. The magnitudes of the stress vectors in some regions have been modified, in order to emphasize the directional aspects of the principal stress. Only the Permalloy layers are shown, since the stress states in only these layers affect domain configurations.

Figure 13 shows the contour mapping of the magnitude of the calculated magnetoelastic energy $K_s = -(3/2)\lambda(S_x - S_y)$. In regions where K_s is greater than K_u , which for Permalloy is equal to +100 J/m³ (1000 ergs/cm³), magnetoelastic effects can influence domain configurations [7]. This fact can be used to predict the tendency for the magnetization direction in the magnetic domains to align with the principal stress direction shown in Figure 12. Influences of head geometries, materials, and process steps on principal stress direction and E_k can then be explored.

6. Electrical and thermal effects in a magnetoresistive head

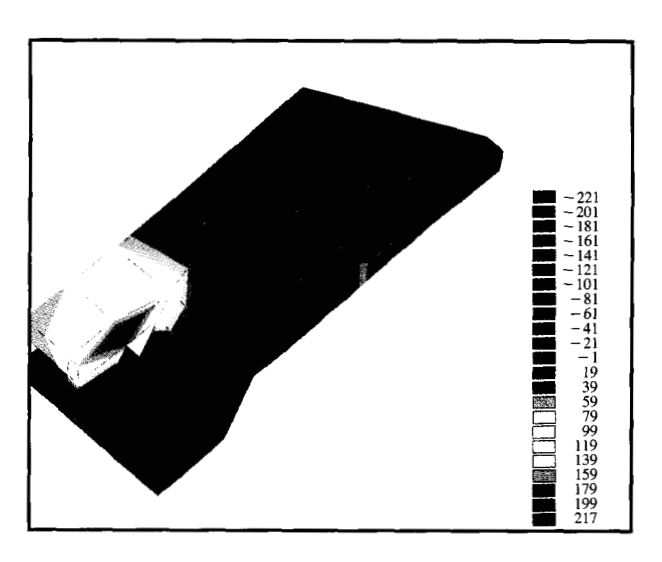
In this section, we discuss the use of finite element calculations involving temperatures in designing a thin-film magnetoresistive (MR) magnetic recording head. An exploded view of the head and leads, sandwiched by the layers from above and below, is shown in Figure 14 (not to scale). Actually, 11 layers are chosen for the device simulation (not just the six shown in Figure 14), from a ceramic substrate to a sputtered alumina overcoat. A symbolic voltage source is shown connected to the leads. The dashed vertical line lies in the symmetry plane that is midway between the leads and perpendicular to the MR stripe. The air bearing surface (ABS) is the shaded area to the front.

For the FEA analysis, an 11-layer mesh is generated, one layer for each layer of the device simulated. The left half of the symmetric structure in Figure 14 is chosen for the calculations and shown in the next three figures. Three-dimensional thermal-electric solid elements are used for the mesh. **Table 2** lists the electrical and thermal material constants used in the analysis. The temperature



Tollife EV

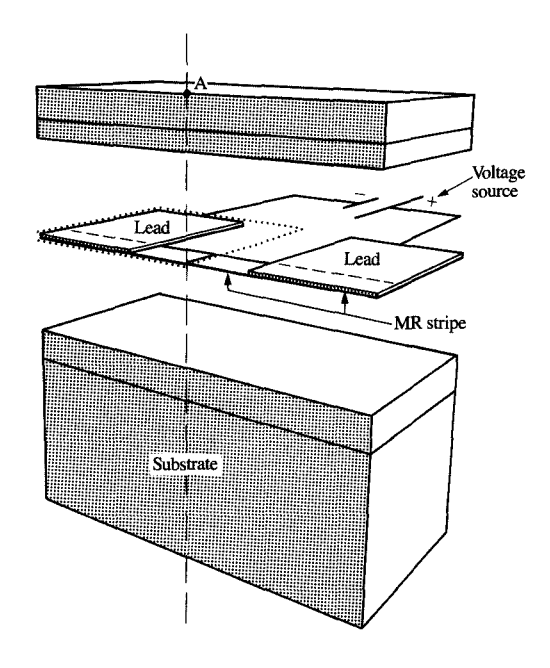
Vector plot of calculated principal stresses in upper half of yoke region of a typical thin-film head, resulting from a uniform temperature change [magnitudes of vectors in back-gap region (see Figure 11) have been reduced].



DISTRICT N

Calculated magnitude of stress anisotropy energy K_s (J/m³) of upper yoke region of thin-film head. $\lambda = 10^{-6}$ (isometric view).

distribution of the head is obtained by first calculating the electrical power (I^2R) joule heating in the MR stripe and leads, and then computing the heat that is conducted



Exploded view of magnetoresistive (MR) head; shaded area is air bearing surface.

Table 2 Electrical and thermal constants of materials used in analyses of Section 6 (3D thermal-electric solid elements).

Material	Electrical resistivity ρ (× $10^{-6} \Omega$ -m)	Thermal conductivity k (W/m/K)
Alumina and substrate	100 000	3.5
MR stripe	$0.25 + 0.0014 \times T^*$	13.0
Shields and leads	0.25	13.0

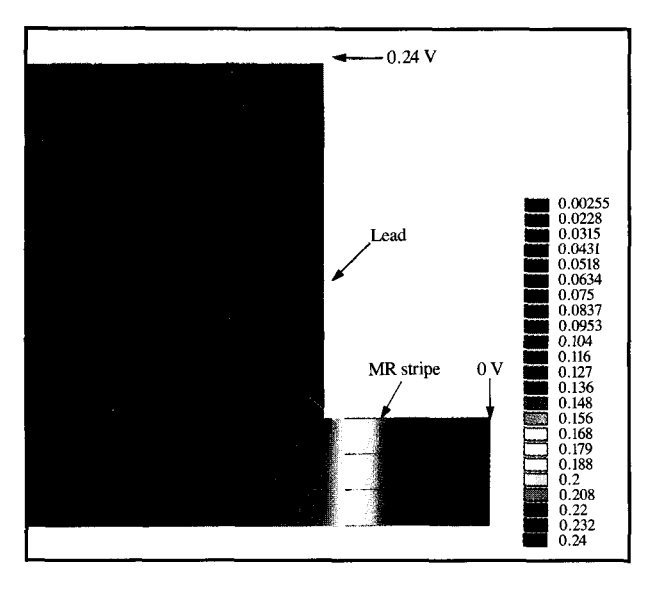
^{*} Nonconstant resistance, T = temperature (K).

away by the surrounding layers to ambient air. Since the joule heating of the MR stripe occurs primarily between the leads, the geometry of the head is modeled precisely in that vicinity. Shape approximations are made farther away from the MR stripe, where structural details have less influence. By extending the mesh in the directions away from the head, we determine that for distances larger than approximately $100~\mu m$, geometric detail has negligible effect upon the calculated temperature distributions. Thus, the volume simulated is truncated, so that it is essentially a $100-\mu m$ cube extending downward, to the left, and to the rear of point A in Figure 14.

The calculation (equation solution part of the FEA) is an iterative process. If the electrical resistivity of the MR stripe were constant, we could (1) apply a voltage across the leads; (2) calculate the equipotentials; (3) calculate the corresponding orthogonal current flow, which depends upon the distribution of electrical resistivities; (4) determine the total current flow through the MR/lead structure; and (5) calculate the required voltage to apply for any desired total current flow. Since the resistivity of the MR stripe is dependent upon temperature, this process must be modified. Steps 2 and 3 become an iterative process. The joule heat generated results in higher temperature and consequently higher resistivity, which must be calculated. The equipotentials and the current flow must be recalculated on the basis of this updated value of resistivity. This in turn causes a change in joule heating. These steps (electrical and thermal calculations) are iterated until the temperature converges, according to a preset convergence criterion. (The metal MR element is not sufficiently nonlinear to lead to thermal instability.) If a particular device requiring a specified current flow is to be simulated, Step 5 is no longer simple. Since the relationship between the voltage and total current is not linear, it is necessary to perform a more global iteration to determine the voltage required for the desired total current through the MR/lead structure. After the initial current is determined, the voltage is adjusted to cause the current to be closer to the desired value. The entire process is iterated until the current is sufficiently close to that value.

Figure 15 shows the resulting equipotentials, as viewed normal to the MR stripe. The part of the mesh shown is the one outlined with the dotted line in Figure 14. (For Figures 15–17, in order to better observe the electrical and thermal behavior in the MR stripe and the neighboring region, we choose a reduced volume to simulate—roughly, a $12-\mu m$ cube. This results in temperatures higher than those for a real head. The full $100-\mu m$ cube is used for the calculation of Figures 18 and 19.) Note that most of the voltage drop occurs across the MR stripe and that the current flow, which is orthogonal to the equipotential lines, is virtually parallel in the region of the MR stripe.

Joule heating produces a temperature distribution that depends on the thermal conduction through the surrounding layers and finally through thermal paths to ambient air, calculated using a film coefficient. This temperature distribution is depicted in **Figure 16**. We find that the highest temperature is at the center of the MR stripe (lower right corner of Figure 16) and closest to the air bearing surface (ABS). The temperature dependence of the MR stripe resistivity ρ , rather than the temperature dependence of the thermal conductivity k of all the layers, is assumed to dominate the nonlinear





Calculated equipotential distribution (V) over MR head and lead, resulting from applied voltage (viewed orthogonally from above).

behavior, because the region of elevated temperature is localized at the MR stripe. In the simulation, the film coefficient (a parameter describing the heat conduction by the ambient air), is adjusted so as to match the calculated with the measured temperatures.

Figure 17 is an isometric view of the temperature distribution of the MR stripe and all of the layers beneath it. From this figure, one can observe how the temperature decreases in all three orthogonal directions.

The dependence of the voltage-current and temperature-current relationships upon head design can be calculated with FEA methods. The temperature-dependent resistance of the MR stripe is illustrated in Figure 18, which shows the applied voltage as a function of the current drawn. The slope of this curve, which is the electrical resistance, increases slightly with increasing current. While the nonlinearity is small, it is significant when these results are applied to electromigration calculations. Figure 18 (as well as Figure 19) shows comparisons of FEA calculations with measurements of this MR head.

The temperature behavior is shown in Figure 19, where the temperature of the MR stripe is plotted against the square of the current. A two-step procedure is used for the temperature measurements. First, as a calibration step, the small-signal resistance of the MR stripe is measured (the low signal current adds negligible heat) while the uniform temperature of the entire MR head, in an oven, is varied over the range of interest. This yields the relationship of temperature and resistance $(V \div I)$.

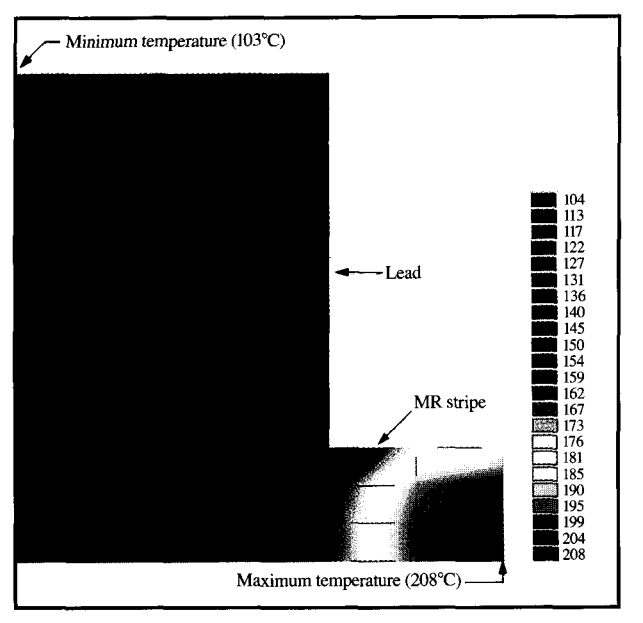


Figure 16

Calculated temperature distribution (°C) over MR head and lead (viewed orthogonally from above). The small volume simulated for this example leads to temperatures higher than those for a real head.

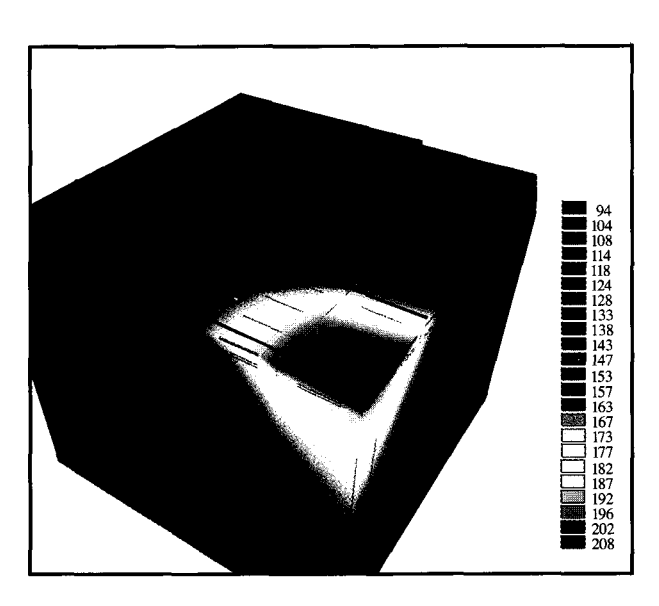
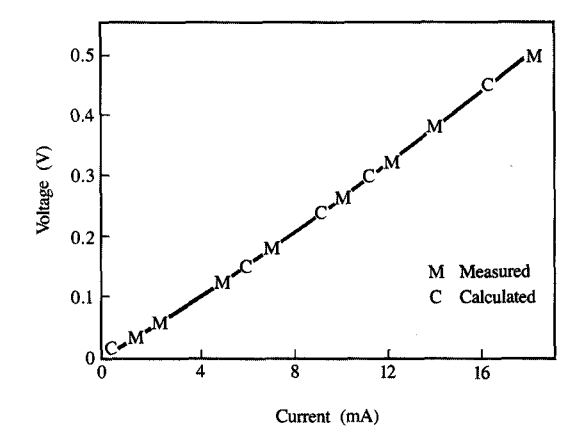
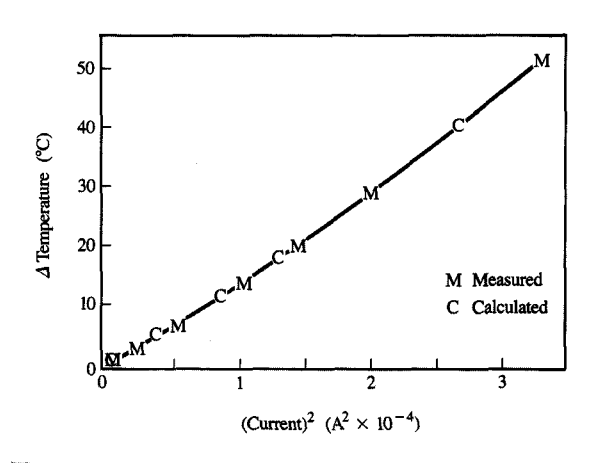


Figure 17

Calculated temperature distribution (°C) over MR head, lead, and lower layers (isometric view).

Then, experimental measurements are made of voltage vs. current (the current in the MR stripe is the entire source of heat), and the temperature is determined, from





Calculated and measured voltage vs. current for MR stripe. Note slight nonlinearity.

Figure 19

Calculated and measured temperature vs. current squared for MR stripe. Note slight nonlinearity.

the calibration results, for the resistance $(V \div I)$ measured. This procedure is valid if the temperature of the MR stripe is uniform. Even with a nonuniform temperature distribution, however, it proves to be very useful as a temperature indicator. To the first order, the temperature shown in Figure 19 is proportional to electrical power (I^2R) . This proportionality to the nonconstant resistance R, however, leads to the same type of nonlinear behavior shown in Figure 18. Comparisons have been made for various head geometries, and the good agreement shown is typical.

The FEA approach allows one to explore the relationship between temperature sensitivities and variations in geometry (e.g., thickness and location of layers) and material properties (e.g., thermal conductivities of materials).

7. Conclusion

Results obtained from computer simulation of the anisotropic stress in simple shapes will be used as building blocks to gain understanding of more complex structures. A thin-film etched slot, rectangular section, and disk are three simple shapes employed in analyzing and calibrating stresses. Three-dimensional anisotropic stress analysis of a thin-film inductive magnetic recording head is described and related to magnetoelastic energy. Electrical and thermal properties of a magnetoresistive (MR) recording head are characterized, including nonlinear electrical resistance effects. Since results can be calculated quickly for many variations of geometries,

material parameters, and boundary conditions, computer simulation can be a very useful tool in analyzing performance and reliability of thin-film devices.

Acknowledgments

I would like to acknowledge the helpful support, discussions, and encouragement of Steven Meeks (Almaden Research), Erik Klokholm (Yorktown Research), and Roy Jensen (SSPD San Jose).

References

- David S. Burnett, Finite Element Analysis, Addison-Wesley Publishing Co., Reading, MA, 1987.
- S. W. Meeks, D. Peter, D. Horne, K. Young, and V. Novotny, "Microscopic Imaging of Residual Stress Using a Scanning Phase-Measuring Acoustic Microscope," *Appl. Phys. Lett.* 55, No. 18, 1835–1837 (1989).
- R. Lacombe, "Stresses in Thin Polymeric Films: Relevance to Adhesion and Fracture," Surface and Colloid Science in Computer Technology, K. Mittal, Ed., Plenum Publishing Co., New York, 1987, pp. 179–197.
- T. Miyauchi, T. Kira, and M. Yoshikawa, "Barkhausen Noise in Yoke Type MR Heads (II)—Inverse Effect of Magnetostriction," IEEE Transl. J. Mag. Jpn. TJMJ-2, No. 7, 609-618 (July 1987).
- H. Koyanagi, R. Arai, K. Mitsuoka, H. Fukui, S. Narishige, and Y. Sugita, "3-D Stress and Magnetic Anisotropy Analysis for Thin Film Heads," *IEEE Transl. J. Mag. Jpn.* 5, No. 2, 185-194 (February 1990).
- K. Young, "Stress in Thin Film Heads: Calculated by the Finite Element Method," Proceedings of Symposium on Magnetic Materials, PV90-8, L. T. Romankiw and D. A Herman, Eds., The Electrochemical Society, Pennington, NJ, 1990, pp. 137-143.
- E. Klokholm and S. Krongelb, "Magnetoelastic Effects In, and Critical Compositions For, Permalloy Thin Film Devices," Proceedings of Symposium on Magnetic Materials, PV90-8, L. T.

Romankiw and D. A. Herman, Eds., The Electrochemical Society, Pennington, NJ, 1990, pp. 125-136.

Received April 4, 1990; accepted for publication August 7, 1990

Kenneth F. Young Storage Systems Products Division, 5600 Cottle Road, San Jose, California 95193. Mr. Young received his B.S. in physics in 1965 from Carnegie Mellon University. He has also done graduate work at the University of Maryland, Georgetown University, and Catholic University. From 1967 to 1978, he worked as a physicist at the National Institute of Standards and Technology, where he was involved in the development of electrical measurements of materials (dielectric properties, dielectric relaxation phenomena, defect centers, and high-temperature ionic conductivity). Mr. Young joined IBM in Kingston in 1978, working there and in Yorktown until 1981 on display device physics, advanced CRT design, and an image quality metric. Since 1981, he has been at IBM San Jose, working on APL programming, ceramics, recording head suspension development, and recording head technology assurance. Mr. Young has been manager of a manufacturing engineering department and instructor of the SSPD "Creative Thinking" class in Los Gatos. Most recently, he has been involved in computer simulation of stress, thermal, and electrical properties of thin-film heads.